Biochimica et Biophysica Acta 1827 (2013) 507–519

Contents lists available at SciVerse ScienceDirect

Biochimica et Biophysica Acta

journal homepage: www.elsevier.com/locate/bbabio

Spectroscopic and functional characterization of cyanobacterium *Synechocystis* PCC 6803 mutants on the cytoplasmic-side of cytochrome b_{559} in photosystem II

Yi-Fang Chiu [a,b,c], Yung-Han Chen [d], Mercedes Roncel [e], Preston L. Dilbeck [f], Jine-Yung Huang [a], Shyue-Chu Ke [d], José M. Ortega [e], Robert L. Burnap [f], Hsiu-An Chu [a,b,*]

[a] *Institute of Plant and Microbial Biology, Academia Sinica, Taipei, 11529, Taiwan*
[b] *Graduate Institute of Biotechnology, National Chung Hsing University, Taichung, 402, Taiwan*
[c] *Molecular and Biological Agricultural Sciences Program, Taiwan International Graduate Program, Academia Sinica, Taiwan*
[d] *National Dong-Hwa University, Hualien, 974-01, Taiwan*
[e] *Instituto de Bioquímica Vegetal y Fotosíntesis, Universidad de Sevilla y CSIC, Américo Vespucio 49, 41092 Seville, Spain*
[f] *Department of Microbiology and Molecular Genetics, Oklahoma State University, Stillwater, OK 74078-4034, USA*

ARTICLE INFO

Article history:
Received 17 November 2012
Received in revised form 18 January 2013
Accepted 30 January 2013
Available online 8 February 2013

Keywords:
Photosystem II
Cytochrome b_{559}
Photoinhibition
Chlorophyll *a* fluorescence
Electron paramagnetic resonance
Thermoluminescence

ABSTRACT

We performed spectroscopic and functional characterization on cyanobacterium *Synechocystis* PCC6803 with mutations of charged residues of the cytoplasmic side of cytochrome (Cyt) b_{559} in photosystem II (PSII). All of the mutant cells grew photoautotrophically and assembled stable PSII. However, R7Eα, R17Eα and R17Lβ mutant cells grew significantly slower and were more susceptible to photoinhibition than wild-type cells. The adverse effects of the arginine mutations on the activity and the stability of PSII were in the following order (R17Lβ > R7Eα > R17Eα and R17Aα). All these arginine mutants exhibited normal period-four oscillation in oxygen yield. Thermoluminescence characteristics indicated a slight decrease in the stability of the $S_3Q_B^-/S_2Q_B^-$ charge pairs in the R7Eα and R17Lβ mutant cells. R7Eα and R17Lβ PSII core complexes contained predominantly the low potential form of Cyt b_{559}. EPR results indicated the displacement of one of the two axial ligands to the heme of Cyt b_{559} in R7Eα and R17Lβ mutant reaction centers. Our results demonstrate that the electrostatic interactions between these arginine residues and the heme propionates of Cyt b_{559} are important to the structure and redox properties of Cyt b_{559}. In addition, the blue light-induced nonphotochemical quenching was significantly attenuated and its recovery was accelerated in the R7Lα and R17Lβ mutant cells. Furthermore, ultra performance liquid chromatography–mass spectrometry results showed that the PQ pool was more reduced in the R7Eα and R17Lβ mutant cells than wild-type cells in the dark. Our data support a functional role of Cyt b_{559} in protection of PSII under photoinhibition conditions in vivo.

1. Introduction

Photosystem II (PSII) is a large membrane protein complex in the thylakoid membrane of plants and cyanobacteria [1–3]. It utilizes light energy to oxidize water on the lumen side and to reduce plastoquinone (PQ) on the stromal-side of the thylakoid membrane [1–3]. Cytochrome (Cyt) b_{559} is one of the essential PSII proteins and is composed of α and β heme-bridged heterodimer proteins (encoded by *psb*E and *psb*F genes, respectively) [1–4]. Previous studies have proposed that Cyt b_{559} participates in secondary electron transfers that protect PSII from photoinhibition forming a cyclic electron-transfer pathway within PSII [5–13]. In these models, Cyt b_{559} is thought to donate its electron, via a β-carotene molecule (Car_{D2}), to reduce highly oxidized chlorophyll

Abbreviations: AL, actinic light; Cyt, cytochrome; Em, erythromycin; E'_m, mid-point redox potential; EPR, electron paramagnetic resonance; F_m, the maximal fluorescence yield; F_{mdark}, the maximal fluorescence yield in the dark; F_o, the dark fluorescence yield; F_v/F_m, the maximal PSII quantum yield [with $F_v = (F_m - F_o)$]; FTIR, Fourier transform infrared; HP, high potential; IP, intermediate potential; LP, low potential; NPQ, nonphotochemical quenching; OCP, orange carotenoid proteins; PQ, plastoquinone; Q_A, the primary quinone electron acceptor in PSII; Q_B, the secondary quinone electron acceptor in PSII; PSII, photosystem II; ROS, reactive oxygen species; UPLC-APCI-QTOFMS, ultra performance liquid chromatography-atmospheric pressure chemical ionization-quadrupole time-of-flight mass spectrometry; Wild-type, control *Synechocystis* strain constructed in the same manner as site-directed mutants but with no mutation; TL, thermoluminescence

* Corresponding author at: Institute of Plant and Microbial Biology, Academia Sinica, Taipei, 11529, Taiwan. Tel.: +886 2 27871169; fax: +886 2 27827954.
E-mail address: chuha@gate.sinica.edu.tw (H.-A. Chu).

0005-2728/$ – see front matter © 2013 Elsevier B.V. All rights reserved.
http://dx.doi.org/10.1016/j.bbabio.2013.01.016

radicals generated in PSII reaction centers under donor-side photoinhibitory conditions [5–10]. On the other hand, Cyt b_{559} may accept an electron from the acceptor side of PSII [Q_B or PQ] to prevent the formation of damaging singlet oxygen species under acceptor-side photoinhibitory conditions [10–14]. In addition, Cyt b_{559} displays different redox potential forms depending on the type of PSII preparation and treatment: a high potential form (HP) with a mid-point redox potential (E'_m) around +390 mV; an intermediate potential form (IP) with an E'_m around +230 mV and a low potential form (LP) with an E'_m about −150–0 mV [5,15,16]. Moreover, recent studies showed that Cyt b_{559} in tris-treated PSII had superoxide oxidase and reductase activities [17,18]. Furthermore, the recent 2.9 Å resolution PSII crystal structure provided evidence that a novel quinone-binding site (Q_C) was located in proximity to Cyt b_{559} [3]. The occupancy of this Q_C site could modulate the redox equilibration between Cyt b_{559} and the PQ pool [19,20] or be involved in the exchange of PQ on the Q_B site [3]. Despite the recent progress in understanding the structure and function of PSII, the exact function of Cyt b_{559} in PSII remains elusive.

Previous target mutagenesis studies demonstrated no stable PSII reaction centers assembled in the absence of either Cyt b_{559} subunit [21–26]. In addition, an early site-directed mutagenesis study with *Synechocystis* PCC6803 showed that replacing either of the heme axial ligands (His22 of the α- or β-subunit) with Leu severely diminished PSII assembly or stability [27]. Furthermore, another site-directed mutagenesis study with *Chlamydomonas reinhardtii* showed that the Cyt b_{559} α subunit mutants His22Tyr and His22Met accumulated 10–15% of PSII (compared to wild-type cells), were sensitive to photoinhibition, and lacked the heme of Cyt b_{559}, while still retaining significant amounts of O_2 evolution activity [28]. This study concluded that a redox role for the Cyt b_{559} heme was not required for O_2 evolution [28]. In our early study, we constructed a set of site-directed mutants of the Cyt b_{559} heme ligands (His22 of the α- or β-subunit) with *Synechocystis* PCC6803 cells [29]. Only the H22Kα mutant grew photoautotrophically and accumulated stable PSII reaction centers [29]. Spectroscopic and functional characterization of the H22Kα and Y18Sα Cyt b_{559} mutant cells showed that both mutants assembled stable PSII and exhibited the normal period-four oscillation in oxygen yield [30]. However, both mutants showed distinct chlorophyll *a* fluorescence characteristics and were more susceptible to photoinhibition than the wild-type [30]. EPR results indicated the displacement of one of the two axial ligands to the heme of Cyt b_{559} in H22Kα mutant reaction centers. In addition, the Y18Sα and H22Kα mutant PSII core complexes predominantly contained the LP form of Cyt b_{559} [30]. When the Cyt b_{559} mutations were placed in a D1-D170A genetic background that prevents Mn cluster assembly, PSII accumulation was almost completely abolished [30]. The results support a functional role of Cyt b_{559} in protection of PSII under photoinhibitory conditions in vivo.

A spontaneously-generated mutant from *Synechocystis* PCC6803 wild-type cells grown in BG-11 agar plates containing 5 mM glucose and 10 μM DCMU was identified as carrying an R7L mutation on the α-subunit of Cyt b_{559} in PSII [31]. This mutant grew at about the same rate as the wild-type cells under photoautotrophical conditions but faster under photoheterotrophical conditions [31]. In addition, the energy delivery from the phycobilisomes to PSII reaction centers was partially inhibited or uncoupled in this mutant. We proposed that the Arg7Leu mutation on the α-subunit of Cyt b_{559} alters the interaction between the allophycocyanin core complex and PSII reaction centers, which reduces energy delivery from the antenna to the reaction center and thus protects mutant cells from DCMU-induced photo-oxidative stress [31].

To gain more insights into the structure and function of Cyt b_{559} in PSII, we performed spectroscopic and functional characterization on *Synechocystis* mutants which carried a mutation on conserved charged residues of the cytoplasmic side of Cyt b_{559} in PSII. The implications of our findings on the structure and physiological functions of Cyt b_{559} in PSII will be discussed.

2. Material and methods

2.1. Growth and preparation of Synechocystis PCC6803 cells

Cyt b_{559} mutant and wild-type *Synechocystis* cells were photoautotrophically grown in BG-11 medium. Cultures were propagated at 30 °C under growth-light conditions with intensity of ~30 μE m^{-2} s^{-1}. Cultures were continuously bubbled with sterile, humidified air. Liquid cultures in exponential growth (OD_{730} 0.7–1.2) were harvested and used for biochemical and functional analysis.

2.2. Construction of Cyt b_{559} mutants

The cytoplasmic-side mutation was introduced into the plasmid PAC559EM^R by oligonucleotide-directed mutagenesis according to reference [29]. Each Cyt b_{559} mutant was constructed by transformation of the mutant plasmid into the host strain (Δ*psb*EFLJ) [29]. Mutants were selected on solid media containing the antibiotic Em (0.1 μg mL^{-1}) until their mutated gene was completely segregated. Complete segregation of the mutated gene in these mutant cells was verified by PCR.

2.3. Measurement of photosynthetic oxygen evolution

Steady-state rates of oxygen-evolution were measured with a Clark-type oxygen electrode (YSI model 5331 oxygen probe) fitted with a water-jacketed cell as described previously [29]. Oxygen evolution of cells (10 μg of chlorophyll mL^{-1}) was measured in growth medium and in the presence of 2 mM 2,6-dichloro-*p*-benzoquinone (DCBQ) and 2 mM potassium ferricyanide as electron acceptor. Oxygen evolution of PSII core complexes was measured in 50 mM MES, pH 6.5, 25 mM $CaCl_2$, 10 mM NaCl, 1 M Sucrose, and in the presence of 1 mM potassium ferricyanide and 0.4 mM DCBQ. Saturating illumination was provided from both sides of the water-jacketed cell by two fiber-optic illuminators (Dolan-Jenner model MI 150).

2.4. Measurement of chlorophyll a fluorescence at 295 K

Chlorophyll *a* fluorescence measurements at 295 K were performed with a Dual PAM (pulse-amplitude-modulation) fluorometer (Walz, Germany). The relative PSII content of cells on a chlorophyll basis was estimated from the total yield of variable chlorophyll *a* fluorescence

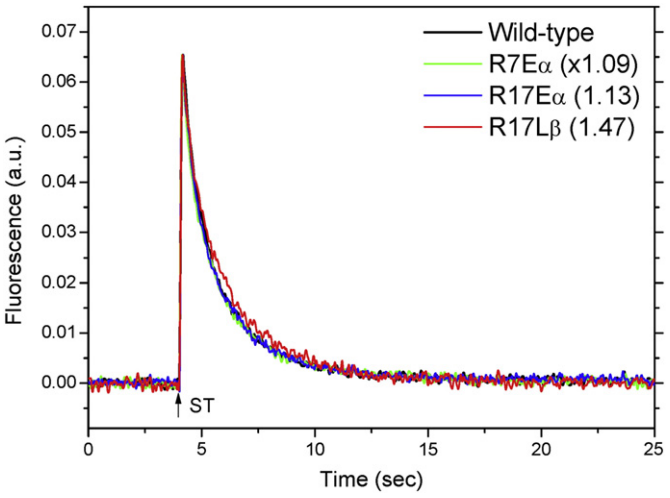

Fig. 1. The kinetics of charge recombination between Q_A^- and PSII electron donors in response to a saturating flash given to the wild-type (black trace), R7Eα (green trace), R17Eα (blue trace) and R17Lβ Cyt b_{559} mutant cells (red trace) in the presence of DCMU, by chlorophyll *a* fluorescence measurement. Conditions: 20 μg of chlorophyll in 2 mL of BG-11 medium. Samples were incubated in darkness for 5 min before DCMU was added to the final concentration of 40 μM. The levels of Fo and Fm were normalized.

($F_m - F_0$) measured in the presence of DCMU and hydroxylamine, according to reference [32]. Experimental conditions for measurements of time-dependent flash-induced transients of PSII fluorescence yield, kinetics of charge recombination between Q_A^- and the Mn cluster, and electron transfer from Q_A^- to Q_B in response to a saturating flash given to the wild-type and mutant cells are described in figure legends. Kinetics of chlorophyll *a* fluorescence decay curves was analyzed using the Microcal Origin 8.1 software implementing two exponential decay fitting [ExpDec2, Equation $y = A1 * \exp(-x/T1) + A2 * \exp(-x/T2)$] of the data in Fig. 1 and three exponential decay fitting [ExpDec3, Equation $y = A1 * \exp(-x/T1) + A2 * \exp(-x/T2) + A3 * \exp(-x/T3)$] of the data in Fig. 2.

2.5. Thermoluminescence measurements

Thermoluminescence (TL) glow curves of *Synechocystis* PCC6803 cells were measured using a home-built apparatus as described earlier [33–35]. Typically, cyanobacterial suspensions were dark-incubated for 3 min at 30 °C, then cooled to 0 °C for 1 min and illuminated at the end of this period with different numbers of saturating single turn-over flashes (separated by 1 s) of white light through an optic fiber. Luminescence emission was recorded while warming samples from 0 °C to 70 °C at a heating rate of 0.5 °C/s. The instrument was driven by a personal computer, with a specially developed acquisition program [36]. Signal analysis and graphical simulation were performed as previously described [33–35]. Statistical analysis of data was done using the Microcal Origin 6.0 software implementing a t-test of the data (see Table 4 and Supplement materials).

2.6. Polarographic measurements of O_2 evolution

Measurement of flash number dependent O_2 yields and O_2 release kinetics was performed with isolated thylakoid membranes using a bare platinum electrode that allows for the deposition of samples by centrifugation as described previously [37–40]. For each measurement a sample of thylakoid membranes containing 3 μg of chlorophyll was added to 500 μL of 50 mM MES-NaOH (pH 6.5), 1 M sucrose, 200 mM NaCl and 10 mM $CaCl_2$. Samples were centrifuged onto the electrode surface at 10,000×*g* for 10 min at 25 °C in a Sorvall HB-4 swing out rotor. The temperature of the electrode was regulated, by circulating thermostatted water through a copper jacket that surrounds the electrode. Acquisition of the data and the control of the instrumentation were implemented using a plug-in data acquisition circuitry and LabView software (National Instruments) that permitted timing and coordination of the flash illumination and data acquisition.

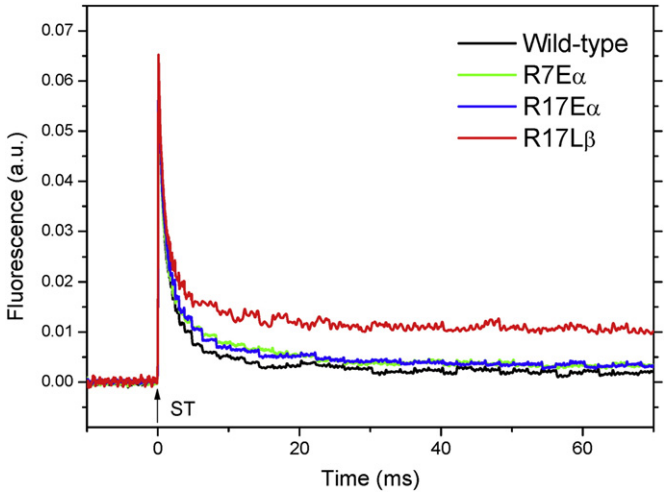

Fig. 2. The kinetics of electron transfer from Q_A^- to Q_B and Q_B^- in response to a saturating flash given to the wild-type (black trace), R7Eα (green trace), R17Eα (blue trace) and R17Lβ Cyt b_{559} mutant cells (red trace) by chlorophyll *a* fluorescence measurement. Conditions: 20 μg of chlorophyll in 2 mL of BG-11 medium. Samples were incubated in darkness for 1 min. The levels of Fo and Fm were normalized.

2.7. Measurement of fluorescence at 77 K

Fluorescence emission spectra were recorded with a fluorescence spectrometer (Jasco model FP-6500). All the measurements were carried out at 77 K, using cell suspensions at a chlorophyll concentration of 20 μg mL^{-1}. The excitation light wavelength used for exciting chlorophyll was 435 nm (excitation band width 5 nm, emission band width 1 nm). The excitation light wavelength used for phycobilisomes was 600 nm (excitation band width 3 nm, emission band width 1 nm).

2.8. Preparations of His-tagged PSII core complexes

Oxygen-evolving His-tagged PSII core complexes were isolated by Ni-NTA affinity chromatography from the wild-type and Cyt b_{559} mutant cells, which contain a His-tag on their CP47 proteins, as described previously [30]. Tris-washed samples were prepared, in accordance with the references cited [30].

2.9. Reduced minus oxidized difference spectra of Cyt b_{559} in the wild-type and mutant PSII core complexes

Optical absorption difference measurements were performed on suspensions of the wild-type and mutant PSII core complexes (20 μg chlorophyll mL^{-1}) in 1 mL MMNB buffer (25 mM MES, 5 mM $MgCl_2$, 10 mM NaCl, 1 M glycine betaine, 0.03% β-DM, pH 5.7) at room temperature, on a Perkin Elmer Lambda 35 UV/VIS spectrophotometer with band width of 0.5 nm. Four-step redox titration was performed as described [30]. The sample suspension was oxidized by adding 0.1 mM $K_3Fe(CN)_6$ (from a freshly made 10 mM stock solution) and the spectrum was recorded and stored as the oxidized spectrum. The sequential reduction of cytochromes was performed by first adding hydroquinone (0.3 mM), followed by ascorbate (0.6 mM) and, finally, a few grains of dithionite.

2.10. Conditions for EPR measurements

EPR spectra were obtained at X-band using a Bruker EMX spectrometer equipped with a Bruker TE102 cavity and an Advanced Research System continuous-flow cryostat (3.2 K–200 K). The microwave frequency was measured with a Hewlett-Packard 5246L electronic counter. The instrument settings are shown in the figure legend.

2.11. Liquid chromatography–mass spectrometry analysis

The relative abundance of PQ and PQH_2 in the wild-type and Cyt b_{559} mutant cells was determined by using ultra performance liquid chromatography-atmospheric pressure chemical ionization-quadrupole time-of-flight mass spectrometry (UPLC-APCI-QTOFMS) technique in accordance with the reference cited [41]. The amount of cells equivalent to 30 mL of $OD_{730} = 1.0$ culture was collected by centrifugation at 10,000×*g* for 2 min and washed with 25 mM HEPES buffer, pH 7.0. The cells were pelleted in a 2 mL microcentrifuge tube. Tetrahydrofuran (THF) solvent and glass beads of about 0.1 mm in diameter were added. Samples were further homogenized for 2 min at 60 Hz in a beadbeater (BioSpec, USA) at 4 °C. Tubes were centrifuged on a benchtop centrifuge (14,000×*g* for 5 min at 4 °C) and 100 μL of supernatant was then transferred to an appropriate glass vial for immediate UPLC-APCI-QTOFMS analysis. The LC–MS system consisted of a Waters Acquity UPLC™ (Waters, USA) coupled to a Waters Synapt HDMS™ system equipped with an atmospheric pressure chemical ionization (APCI) source. Prenyllipids were separated on an Acquity BEH C18 column (50×2.1 mm, 1.7 μm) as described previously [41].

3. Results

3.1. Growth and photosynthetic characteristics of Cyt b_{559} mutants

A new set of site-directed Cyt b_{559} mutants, each one carrying a single amino acid substitution on the charged residues (Glu6, Arg7, Asp11 and Arg17 of the α subunit and Arg17 of the β subunit) situated on the cytoplasmic side of Cyt b_{559}, was constructed in the experimental model cyanobacterium *Synechocystis* PCC 6803. The light-saturated oxygen-evolution activity and PSII contents of the mutant strains that are discussed in this study are listed in Table 1. All these mutant cells grew photoautotrophically, although the growth rates of the R7Eα, R17Eα and R17Lβ cells were significantly slower than that of the WT cells. Under photoautotrophic growth conditions, the doubling times for the wild-type, R7Eα, R17Eα and R17Lβ Cyt b_{559} cells were about 14.2, 24.4, 19.5 and 30.7 h, respectively.

The maximal oxygen evolution rates and PSII content of the E6Rα, R7Eα, D11Rα and R17Eα mutant cells were about 57–65% and 53–75% compared to that of the wild-type cells, respectively (Table 1). In contrast, the oxygen evolution rates and PSII contents were less affected in the E6Aα, R7Aα, R7Lα, D11Aα and R17Aα mutant cells (see Table 1). Therefore, our results indicated that the replacement of the charged amino acid residue with the oppositely charged residue on the cytoplasmic side of Cyt b_{559} mutants had larger impacts on their PSII stability and activity than replacements with the neutral residues. Exceptionally, among all the cytoplasmic-side Cyt b_{559} mutants in Table 1, the R17Lβ mutant cells showed the lowest oxygen evolution activity (29% compared to that of the wild-type cells) and PSII content (41% of the wild-type cells). Our results indicated that the mutation on the R17β residue had the strongest impacts on PSII activity and stability among all charged residues on the cytoplasmic side of Cyt b_{559} in PSII.

3.2. Measurement of chlorophyll a fluorescence at 295 K

Fig. 1 shows the charge recombination kinetics between Q_A^- and oxidized PSII electron donors in the wild-type, R7Eα, R17Eα and R17Lβ mutant cells as measured by chlorophyll *a* fluorescence. The decay kinetics was analyzed assuming two exponentially decaying components and listed in Table 2. The charge recombination kinetics of the wild-type cells exhibited components of T1 ~ 0.68 s (50%), T2 ~ 2.36 s (50%) and reflects charge recombination between Q_A^- and the S_2 state of the Mn cluster [32,42]. The R7Eα and R17Eα mutant cells showed similar kinetics of charge recombination compared to that of the wild-type cells. These results indicate that the Mn cluster and Q_A are generally intact in PSII of these mutant cells. However, the R17Lβ mutant cells showed a slight alteration in relative amplitudes of components [T1 ~ 0.59 (38%) and T2 ~ 2.57 s (62%)] compared to those of the wild-type cells. In addition, the flash-induced yields of variable chlorophyll *a* fluorescence in the R7Eα, R17Eα and R17Lβ mutant cells were about 92%, 88% and 68% of the wild-type cells, respectively (see Fig. 1). Fig. 2 and Table 3 show kinetics of Q_A^- oxidation in response to a saturating flash given to the wild-type and Cyt b_{559} mutant cells in the absence of DCMU. The fast phase, which contributes to ~52% of the total decay with T1 ~ 0.44 ms in the wild-type cells (Table 3), reflects the electron transfer from Q_A to Q_B (or Q_B^-) with occupied PQ binding site [43,44]. The middle phase [T2 ~ 2.8 ms (41%)] reflects the electron transfer from Q_A to Q_B with the empty PQ binding site [43,44]. The slow phase [T3 ~ 71 ms (7%)] may reflect that the site is temporarily blocked by the presence of Q_BH_2 [43]. The slower time constant of the fast and middle phases in the R7Eα and R17Lβ mutant cells indicates slower electron transfer from Q_A to Q_B in their PSII. In addition, the time constant (T3 ~ 510 ms) of the slow phase in the R17Lβ mutant cells was much slower relative to wild-type and could be attributed to $S_2Q_A^-$ charge recombination [42–44]. The relative amplitude of the slow phase (~19%) in R17Lβ cells was also larger than that of wild-type (~9%). Our results suggest that the R17Lβ mutant cells may contain a significant fraction of inactive PSII reaction centers. The other mutant cells, listed in Table 1, all showed similar electron transfer from Q_A^- to Q_B and Q_B^- as for the wild-type cells (data not shown).

Table 1
Summary of the properties of cytoplasmic side Cyt b_{559} mutants.

Strains	Oxygen evolution[a] (% of wild-type)	PSII content[b] (% of wild-type)	
Wild-type	100 ± 7	100 ± 10	
E6Aα	75 ± 11	86 ± 4	
E6Rα	65 ± 8	69 ± 2	
R7Kα	87 ± 5	89 ± 2	
R7Aα	70 ± 9	72 ± 7	
R7Lα	69 ± 13	84 ± 2	Ref. [31]
R7Eα	57 ± 9	53 ± 6	
D11Aα	91 ± 9	98 ± 8	
D11Rα	65 ± 8	75 ± 10	
R17Aα	81 ± 9	86 ± 1	
R17Eα	64 ± 5	64 ± 4	
R17Kβ	61 ± 8	62 ± 11	
R17Lβ	29 ± 1	41 ± 8	

[a] The average O_2 evolution rate of wild-type cells was 518 ± 38 μmol O_2 mg Chl^{-1} h^{-1}.
[b] Estimated from the total yield of variable chlorophyll *a* fluorescence ($F_m - F_o$).

Table 2
Kinetics of charge recombination between Q_A^- and oxidized PSII electron donors in response to a saturating flash given to the wild-type and Cyt b_{559} mutant cells in the presence of DCMU.

Strain	Fast phase T1 (s)/Amp (%)	Slow phase T2 (s)/Amp (%)
Wild-type	0.68 ± 0.02/50	2.36 ± 0.03/50
R7Eα	0.59 ± 0.01/48	2.42 ± 0.03/52
R17Eα	0.56 ± 0.01/45	2.26 ± 0.02/55
R17Lβ	0.59 ± 0.02/38	2.57 ± 0.03/62

The data were obtained from the analysis of the fluorescence relaxation curves shown in Fig. 1 by using the function described in the Material and methods.

3.3. Thermoluminescence characteristics

Excitation of cell suspensions of WT and Cyt b_{559} mutants with a series of saturating single turn-over flashes at 0 °C induced the appearance of very complex TL glow curves. The light emission curves obtained after illumination with two flashes were the greatest of the series and are shown in Fig. 3. These TL signals could be well simulated by two decomposition components that we assigned to the B1 and B2 bands originating from the recombination of $S_3Q_B^-$ and $S_2Q_B^-$ charge pairs, respectively [45]. The results show that the amplitude of the signals of the B-bands ($S_3Q_B^-/S_2Q_B^-$) of the R7Lα, R7Eα, R17Aα and R17Lβ mutants is smaller than that of wild-type, especially of the R7Eα and R17Lβ mutants. The results are roughly correlated with the estimated PSII contents in these mutant cells by variable chlorophyll *a* fluorescence measurement in Table 1, although the yield of TL is complicated by other factors [45,46]. In addition, the T_{max} of the B1 and B2 bands for the wild-type and the different

Table 3
Kinetics of Q_A^- oxidation in response to a saturating flash given to the wild-type and Cyt b_{559} mutant cells in the absence of DCMU.

Strain	Fast phase T1 (ms)/Amp (%)	Middle phase T2 (ms)/Amp (%)	Slow phase T3 (ms)/Amp (%)
Wild-type	0.44 ± 0.01/52	2.79 ± 0.02/41	71 ± 1/7
R7Eα	0.66 ± 0.01/68	6.52 ± 0.05/24	161 ± 4/8
R17Eα	0.52 ± 0.01/54	3.45 ± 0.02/37	104 ± 1/9
R17Lβ	0.78 ± 0.01/63	5.90 ± 0.09/18	513 ± 16/19

The data were obtained from the analysis of the fluorescence relaxation curves shown in Fig. 2 by using the function described in the Material and methods.

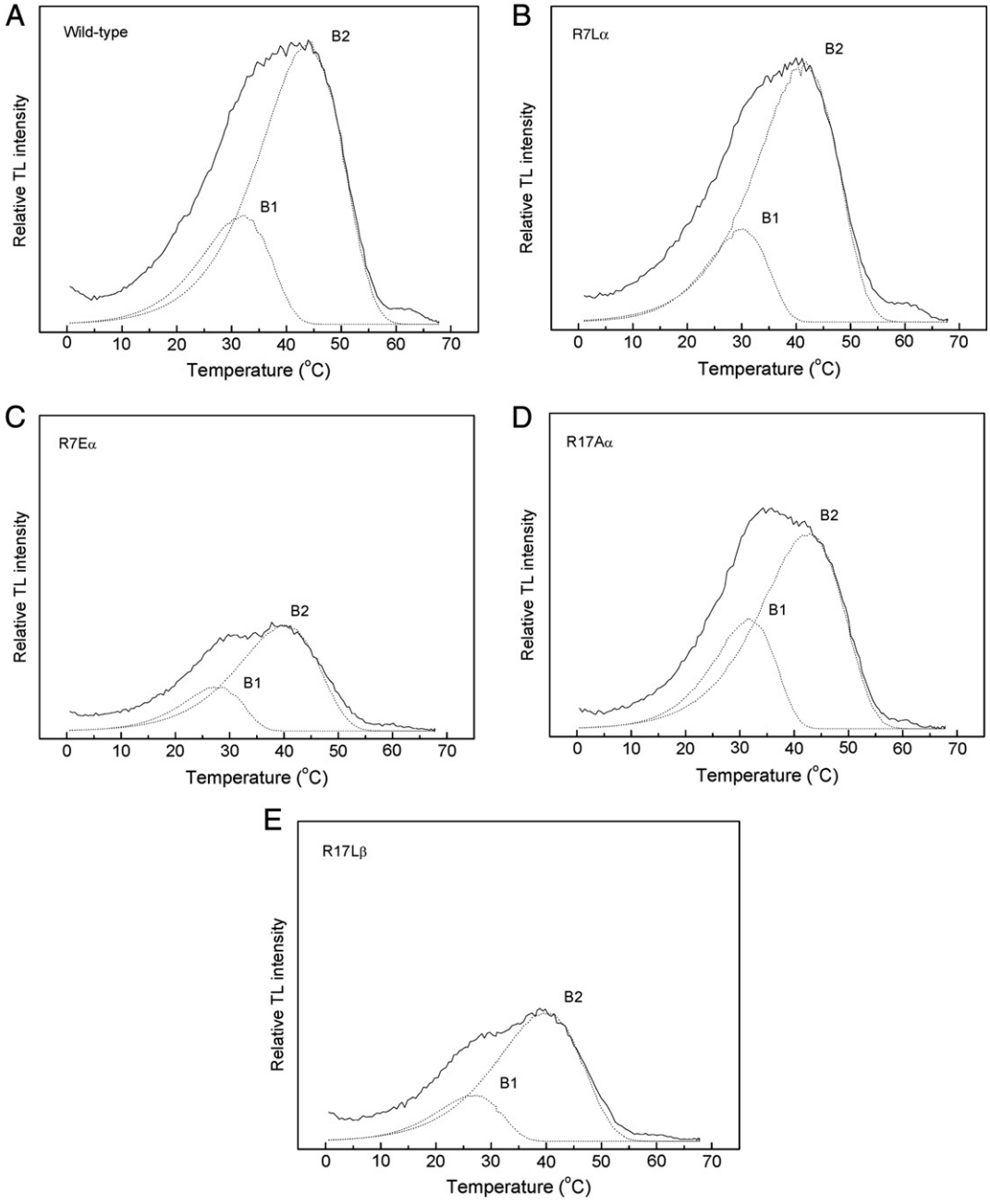

Fig. 3. Thermoluminescence glow curves (B bands) of the (A) wild-type, (B) R7Lα, (C) R7Eα, (D) R17Aα, and (E) R17Lβ Cyt b_{559} mutant cells recorded after two flashes. The dashed lines represent the simulation components (B1-band and B2-band) corresponding to the best fit (see Material and methods). All measurements were carried out using cells centrifuged and resuspended in a 40 mM MES (pH 6.5) buffer at a chlorophyll concentration of 50 μg mL^{-1}.

mutants were calculated (Table 4). For the R7Lα and R17Aα mutants these values were very similar to that of the wild-type cells (T_{max} at 31 °C for B1-band and 43 °C for B2-band). However, the T_{max} of the B1-band ($S_3Q_B^-$) and B2-band ($S_2Q_B^-$) of the R7Eα and R17Lβ mutants show a small but significant downshift (2–3 °C) in comparison to that of the wild-type cells (see statistical analysis in Supplement materials). The small down-shift of the T_{max} of B-bands in the R7Eα and R17Lβ mutant cells indicates a slight decrease in the stability of the $S_3Q_B^-/S_2Q_B^-$ charge pairs in these mutant cells. Since the T_{max} of both B1 and B2 bands change in the same direction and the two recombination pairs have the same acceptor (Q_B^-) and different donor (S_3 and S_2) components, our results suggested that the R7Eα and R17Lβ mutations exerted a small but significant effect on the acceptor side of PSII (Q_B^-). Furthermore, there was no significant change in the oscillation patterns of the B-band amplitude with the number of flash in these Cyt b_{559} mutant cells (see Fig. S1). However, we cannot exclude the possibility that the small changes in the extent of the B-band shift might also reflect alterations in the frequency of occupation of reduced PQ in the Q_B site during the measurements due to differences in the redox level of the PQ pool in these mutants (see below).

Table 4
The peak position of the B-bands in the wild-type, R7Lα, R7Eα, R17Aα and R17Lβ cells. Each value is the average of the estimated values from the TL curves of 7–11 independent experiments.

	Wild-type	R7Lα	R7Eα	R17Aα	R17Lβ
B1 band	31 ± 2 °C	31 ± 2 °C	29 ± 3 °C	30 ± 2 °C	29 ± 2 °C
B2 band	43 ± 1 °C	42 ± 1 °C	40 ± 1 °C	42 ± 2 °C	40 ± 2 °C

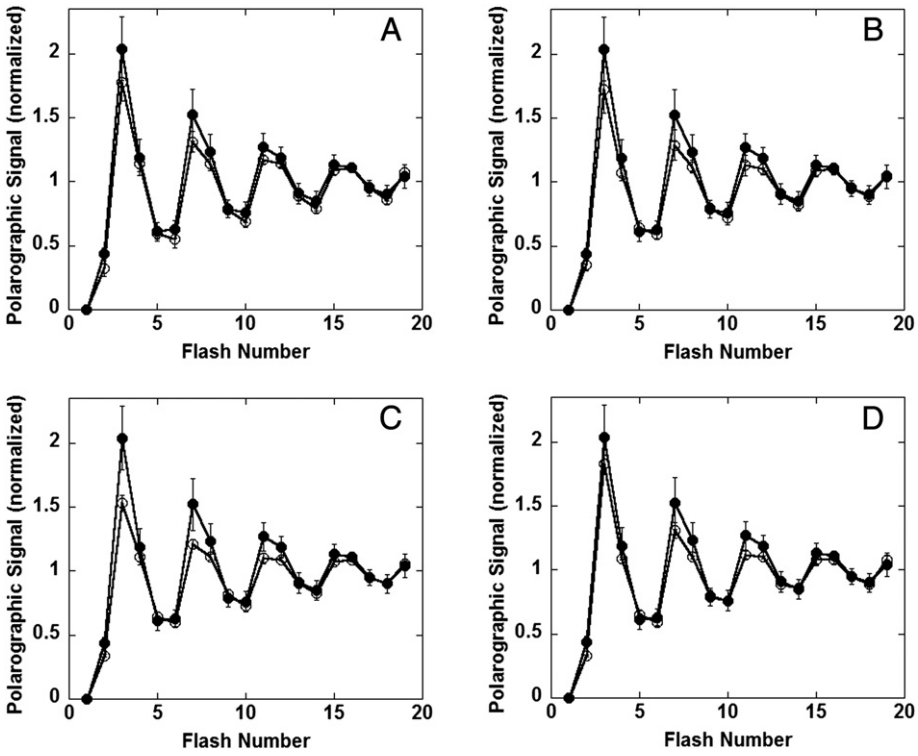

Fig. 4. Flash dependent O_2 yields from thylakoid membranes. The wild type (closed circles) and R7E (Panel A), R7Lα (Panel B), R17A (Panel C) and R17Lβ (Panel D) mutant (open circles) thylakoid membranes were centrifugally deposited onto the surface of a bare platinum electrode. The flash dependent O_2 yields were then measured from a series of 20 actinic flashes from a xenon flash lamp given at 4 Hz. The signal amplitudes were normalized to the average amplitude of the last four flashes. Each trace represents the averaged peak amplitudes from 3 samples with error bars representing the standard deviation.

3.4. Oxygen-flash yield experiment

Fig. 4 shows the patterns of flash number dependent oxygen yield on the dark-adapted Cyt b_{559} mutant and wild-type thylakoid membranes which were measured on a bare platinum electrode under a sequence of saturating, single-turnover flashes given at a frequency of 4 Hz. All mutants exhibited the fairly normal period-four oscillation in oxygen yield (Fig. 4). The oscillatory patterns were analyzed using an eigenvector method to estimate the parameters α, β, and γ, which correspond to misses, hits, and double hits, respectively. These results are summarized in Table 5. Our results showed that only relatively small alterations in the transition probabilities in these Cyt b_{559} mutant cells were detected with this analysis again indicating that the mutations have minimal impact upon the donor side of PSII.

3.5. Determination of different midpoint potential forms of Cyt b_{559} in the wild-type and mutant PSII core complexes

To estimate the potential forms of Cyt b_{559} in the wild-type and mutant PSII core complexes, reduced-minus-oxidized optical difference spectra of the Cyt b_{559} heme in the wild-type and Cyt b_{559} mutant oxygen-evolving PSII core complexes were measured (Fig. S2). The HP and IP forms of Cyt b_{559} were estimated by the hydroquinone-reduced minus ferricyanide-oxidized and the ascorbate-reduced minus hydroquinone-oxidized absorption difference spectra, respectively. Dithionite-reduced minus ascorbate-oxidized absorption difference spectra contain both the LP forms of Cyt b_{559} and Cyt c_{550} (Fig. S3). Because Cyt c_{550} does not contribute significantly at 559.5 nm of the difference spectra, we used the amplitude of dithionite-reduced minus ascorbate-oxidized absorption difference spectra at 559.5 nm to estimate the content of the LP form of Cyt b_{559}. The wild-type PSII core complexes contained ~8% HP form, ~78% IP form and ~14% LP form of Cyt b_{559} (see Table 6 and Fig. S2A). In contrast, the R7Eα and R17Lβ PSII core complexes contained predominantly LP form (72% and 78%, respectively) and less IP form and HP form of Cyt b_{559} (see Table 6; Fig. S2B and S2E). In the R17Aα and R17Eα PSII core complexes, the amount of IP form (~49%) of Cyt b_{559} was slightly higher than that of LP form (~46% and ~41%, respectively) of Cyt b_{559} (see Table 6; Fig. S2C and S2D). Our results demonstrated that the proportion of the different redox potential forms of Cyt b_{559} was significantly altered in these mutant PSII core complexes, presenting the R7Eα and R17Lβ mutations of Cyt b_{559} the greatest effect.

Table 5
S-state cycling parameters. Estimation of S-state parameters was performed using a four state model as previously described [47,48]. Each value is the average of the estimated values from the fits of three individual measurements. All standard deviations are less than 6%.

Strain	S_0	S_1	S_2	S_3	Misses, α	Hits, β	Double hits, δ
Wild-type	21.4	66.6	12.0	0.0	10.3	87.7	2.0
R7Lα	23.5	61.1	12.7	2.7	11.8	86.2	2.0
R7Eα	25.0	65.1	9.8	0.2	10.7	87.3	2.0
R17Aα	28.4	59.5	12.1	0.0	12.0	86.0	2.0
R17Lβ	19.9	69.8	10.3	0.0	12.3	85.7	2.0

Table 6
Summary of properties of Cyt b_{559} mutant PSII core complexes.

Strains	Oxygen evolution (μmol O_2 mg Chl^{-1} h^{-1})	Redox potential forms		
		HP	IP	LP
Wild-type	3010	8%	78%	14%
R7Eα	1500	6%	22%	72%
R17Aα	2910	5%	49%	46%
R17Eα	2250	10%	49%	41%
R17Lβ	1300	0%	22%	78%

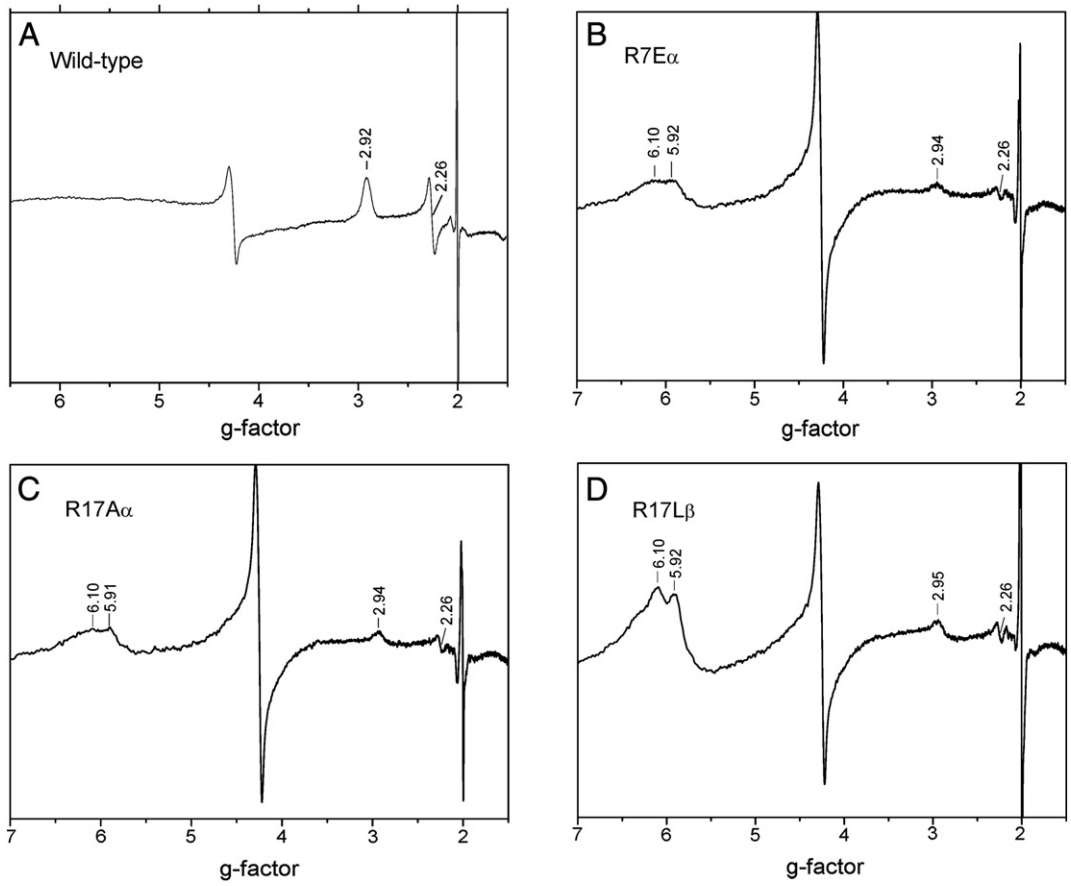

Fig. 5. The EPR spectra of Cyt b_{559} heme in the oxygen-evolving (A) wild-type, (B) R7Eα, (C) R17Aα, and (D) R17Lβ mutant PSII core complexes. EPR conditions: microwave frequency, 9.54 GHz; modulation amplitude, 20 G at 100 kHz; temperature, about 10 K; microwave power, 20 mW.

3.6. EPR spectroscopy

Fig. 5 shows EPR spectra of Cyt b_{559} from the oxygen-evolving R7Eα, R17Aα and R17Lβ mutant PSII core complexes. The wild-type PSII core complexes gave rise to EPR signals of the low-spin heme of cytochromes ($g_z = 2.92$; $g_y = 2.26$), which were contributed from both Cyt b_{559} and Cyt c_{550} [29,30]. In contrast, the R7Eα, R17Aα and R17Lβ mutant PSII core complexes gave rise to EPR signals which are characteristic for both the low-spin heme of cytochromes ($g_z \sim 2.94$; $g_y = 2.26$) and also the high-spin heme of Cyt b_{559} ($g_z \sim 6.10$; $g_y \sim 5.92$) [29,30]. Moreover, under 77 K illumination, the wild-type PSII core complexes gave rise to additional EPR signals ($g_z = 3.05$; $g_y = 2.17$) that were contributed from photooxidation of HP and some IP form of Cyt b_{559} (data not shown) [29,30]. In contrast, there are no significant light-induced EPR signals for photo-oxidization of HP or IP form of Cyt b_{559} in the R7Eα, R17Aα and R17Lβ mutant PSII core complexes under 77 K illumination (data not shown). Continuous-wave–EPR spectral characterizations of Cyt b_{559} from the Tris-washed PSII core complexes of the (A) wild-type, (B) R7Eα, (C) R17Aα, and (D) R17Lβ Cyt b_{559} mutants were shown in Fig. S4. The Tris-washed PSII core complexes were depleted of manganese ions and extrinsic polypeptides, including Cyt c_{550} [30]. EPR signals characteristic of the low spin heme of Cyt b_{559} ($g_z = 2.98$; $g_y = 2.25$) were obtained for the Tris-washed wild-type PSII core complexes. In contrast, the Tris-washed R7Eα and R17Lβ mutant PSII core complexes gave rise to EPR signals for the high spin heme of Cyt b_{559} ($g_z \sim 6.10$; $g_y = 5.89$) and the Tris-washed R17Aα mutant PSII core complexes showed signals for both the low ($g_z = 2.92$; $g_y = 2.26$) and the high ($g_z = 6.11$; $g_y = 5.89$) spin heme of Cyt b_{559}.

3.7. 77 K-fluorescence emission spectra

Fig. 6A shows the 77 K-fluorescence emission spectra recorded from cells that were excited at 600 nm, where phycobilin pigments preferentially absorb. The wild-type cells gave rise to the emission peaks at ~648 nm (from phycocyanin), ~655 nm (from allophycocyanin) and at ~690 nm (from PSII) [49–51]. In the spectra of the R7Eα, R17Aα, R17Eα and R17Lβ Cyt b_{559} mutant cells, the emission peak from allophycocyanin was significantly shifted to ~656 nm and the other peak was strongly enhanced and shifted to ~686 nm. The emission peaks at ~686 nm originated from terminal phycobilin emitters (ApcE). Therefore, the enhancement of emission peaks at 686 nm in the R7Eα, R17Aα, R17Eα and R17Lβ Cyt b_{559} mutant cells indicated that the energy transfer from the phycobilisomes to PSII reaction centers was significantly inhibited or uncoupled in these mutant cells.

Fig. 6B shows the 77 K-fluorescence emission spectra recorded from cells excited at 435 nm, where the chlorophyll molecule preferentially absorbs. In the spectra of the wild-type and Cyt b_{559} mutant cells, preferential excitation of chlorophyll at 435 nm resulted in three emission peaks: at ~685, ~693 and ~720 nm. According to previous studies, the emission peak at ~685 nm is originated from CP43 or from terminal phycobilin emitters (ApcE) [49–52] and the peaks at ~693 nm and ~720 nm are derived from functional PSII and PSI reaction centers, respectively ([49–52] and the references therein). Therefore, the diminishment of the emission peaks at ~693 nm in the spectra of the R7Eα, R17Eα and R17Lβ Cyt b_{559} mutant cells was correlated with their lower content of PSII compared to the wild-type and R17Aα mutant cells (see Table 1).

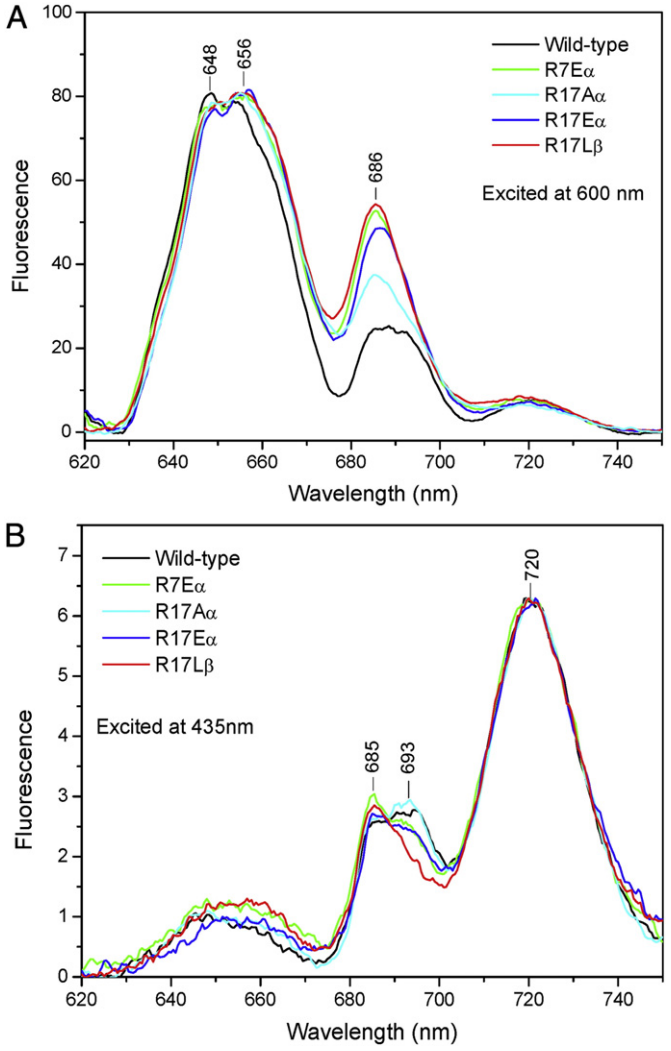

Fig. 6. 77 K-fluorescence emission spectra from the wild-type, R7Eα, R17Aα, R17Eα and R17Lβ mutant cells. (A) Excited phycobilisomes at 600 nm (the spectra were normalized at 656 nm). (B) Excited chlorophyll at 435 nm (the spectra were normalized at 720 nm). All measurements were carried out at 77 K, using cell suspensions at a chlorophyll concentration of 20 μg mL^{-1}.

3.8. PSII fluorescence yield in the presence and absence of actinic light

The R7Eα, R17Eα and R17Lβ mutant cells showed very distinct time-dependent flash-induced transients of PSII fluorescence yield in the presence and absence of actinic light as compared with the wild-type cells (see Fig. 7). The wild-type cells showed the lowest F_o (0.13 ± 0.01) and the highest F_v/F_{mdark} (0.42 ± 0.04). The F_v/F_{mdark} parameter is a measure of maximal PSII quantum yield in dark-adapted cells (with $F_v = F_{mdark} - F_o$). In contrast, all mutant cells showed the high F_o (0.25 ± 0.02 for R7Eα; 0.18 ± 0.04 for R17Eα; 0.25 ± 0.02 for R17Lβ) and low F_v/F_{mdark} values (0.27 ± 0.02 for R7Eα; 0.32 ± 0.07 for R17Eα; 0.15 ± 0.01 for R17Lβ) as compared with the wild-type cells. In addition, the maximal fluorescence yield (F_m) induced by periodic saturating pulses in Cyt b_{559} mutant cells was significantly increased during the actinic light illumination and then decreased after the actinic light was turned off. In contrast, the F_m value for the wild-type cells remained almost constant before, during, and after actinic light illumination. The results can be attributed to the changes in maximal fluorescence yield that accompany with state transitions ([53,54] and the references therein) and the fluorescence emission from uncoupled phycobilisomes in mutant cells.

In the dark-adapted wild-type cells, the fluorescence yield decayed back to the F_o level rapidly after the excitation of the multiple-turnover saturating pulse. In contrast, in the dark-adapted R7Eα, R17Eα and R17Lβ mutant cells, the fluorescence yield decayed back to the F_o level initially and then rose to a level slightly higher than F_o and decayed back again to F_o. This effect was not observed in the R7Eα, R17Eα and R17Lβ mutant cells under the actinic light (Fig. 7) or under the far-red light (see Fig. S5).

Furthermore, the maximal PSII quantum yield (F_v/F_m) after the actinic light illumination was significantly decreased compared to the F_v/F_{mdark} in the R7Eα, R17Eα and R17Lβ mutant cells. In contrast, the F_v/F_m value after the actinic light illumination was about the same as the F_v/F_{mdark} value in the wild-type cells (Fig. 7). Our results suggested that a significant fraction of PSII were photo-inhibited in the R7Eα, R17Eα and R17Lβ mutant cells but not in the wild-type cells under our experimental conditions. Moreover, the steady-state oxygen-evolution rates were also decreased faster in these mutant cells than in the wild-type under the high light condition (Fig. S6).

Fig. 8 shows the effects of blue light-induced nonphotochemical quenching (NPQ) in the wild-type and Cyt b_{559} mutant cells. When the wild-type cells were illuminated with 220 μE m^{-2} s^{-1} blue actinic light, a strong quenching in their fluorescence yields was induced and the steady-state fluorescence (F_s) levels dropped below the F_o level during the blue actinic light illumination (Fig. 8A). Once blue actinic light was turned off, the F_m' and F_o' recovered slowly back to the initial level in the dark. In contrast, the effects of blue light-induced NPQ were less apparent in the R7Lα and R17Lβ mutant cells under the same experimental conditions (Fig. 8B, C). When the higher intensity (~350 μE m^{-2} s^{-1}) of the blue actinic light was applied, the effects of blue light-induced NPQ were further enhanced in the wild-type cells (Fig. 8D). Under the high blue light illumination (~350 μE m^{-2} s^{-1}), the R7Lα and R17Lβ mutant cells also showed significant blue-light-induced NPQ (Fig. 8E and F). Interestingly, when the blue actinic light was turned off, the recovery of NPQ in the R7Lα and R17Lβ mutant cells was significantly faster than that of wild-type cells. After the blue light was turned off for 300 s, the F_m' and F_o' values in both the R7Lα and R17Lβ mutant cells almost returned to their initial levels (F_{mdark} and F_o), whereas the F_m' and F_o' values for the wild-type cells were still significantly lower than the F_{mdark} and F_o values. Our results indicated that the effects of blue light-induced NPQ were significantly attenuated and the recovery of blue light-induced NPQ was accelerated in the R7Lα and R17Lβ Cyt b_{559} mutant cells.

3.9. The redox state of PQ pool

To determine the redox state of PQ pool in the wild-type and Cyt b_{559} mutant cells, we used the UPLC-APCI-QTOFMS method to measure the relative abundance of PQ and PQH_2 [41]. This method was developed recently for the rapid and simultaneous profiling of prenylquinones in plant tissues by ultra-high pressure liquid chromatography–mass spectrometry [41]. We found that the PQH_2/PQ_{tot} ratio was about 0.38 ± 0.04 for the dark-adapted wild-type cells (see Fig. 9 and Fig. S7). In contrast, the PQH_2/PQ_{tot} ratio was about 0.51 ± 0.02 and about 0.61 ± 0.01 for the dark-adapted R7Eα and R17Lβ Cyt b_{559} mutant cells, respectively (see Fig. 9). Our results demonstrated that the redox state of PQ pool in the dark was more reduced in the R7Eα and R17Lβ Cyt b_{559} mutant cells than in the wild-type cell.

4. Discussion

4.1. Cytoplasmic-side arginine residues are important to the structure and redox properties of Cyt b_{559} in PSII

In this work, we performed spectroscopic and functional characterization on Cyt b_{559} mutants which carried a mutation on the

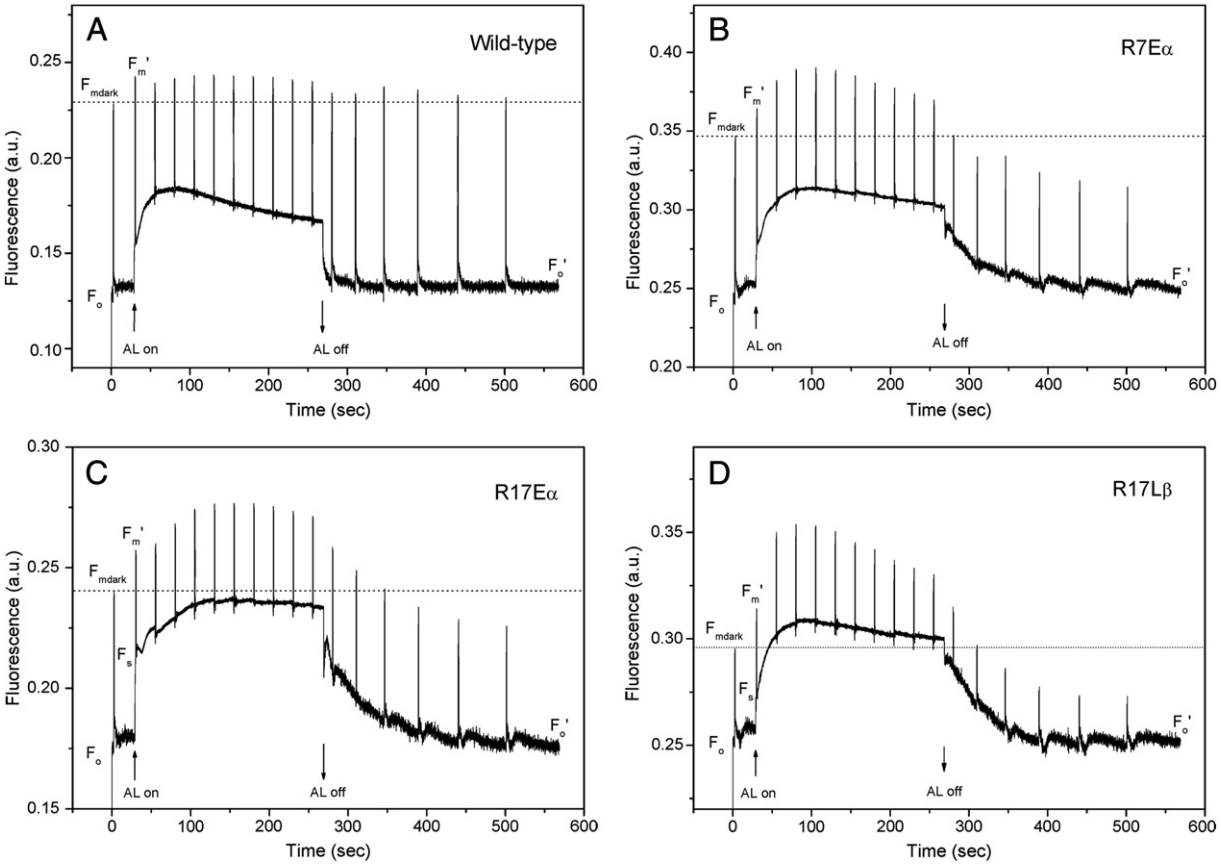

Fig. 7. Time-dependent flash-induced fluorescence yield of the (A) wild-type, (B) R7Eα, (C) R17Eα, and (D) R17Lβ mutant cells in the presence and absence of red actinic light. The intensity of the red actinic light was about 40–50 μE m^{-2} s^{-1}.

charged residues (Glu6, Arg7, Asp11 and Arg17 of the α subunit and Arg17 of the β subunit) on the cytoplasmic side of Cyt b_{559} in the cyanobacterium *Synechocystis* PCC6803. These charged residues on the cytoplasmic side of Cyt b_{559} are highly conserved in higher plants and cyanobacteria [55]. Mutations at Arg7 and Arg17 of the α subunit and Arg17 of the β subunit on the cytoplasmic side had a relatively large effect on the activity and stability of PSII in the mutant cells, especially with R7Eα, R17Eα, and R17Lβ mutations (see Table 1). The R7Eα, R17Eα, and R17Lβ mutant cells still retained the ability to grow photoautotrophically, but their photosynthetic growth and oxygen evolution rates were significantly slower than the wild-type cells. The high resolution crystal structure of PSII revealed that the side chain of R17β lies close enough to form a hydrogen bond or salt bridge with the D-propionate of the heme in Cyt b_{559}; the side chains of R7α and R17α may interact with the A-propionate of the heme in Cyt b_{559} [1,3]. These arginine residues may also function to modulate the ionization state of the nearby heme propionate and influence the redox potential of the heme [56]. Therefore, these conserved arginine residues on the α- and β-subunits of Cyt b_{559} may play important roles in the structure and redox properties of the heme in Cyt b_{559}. In addition, the impact of these arginine mutations on the structure and stability of PSII was generally in the order of R17Lβ > R7Eα > R17Eα and R17Aα. Because both the side chains of the Arg 7 and Arg17 residues on the α-subunit of Cyt b_{559} interact with the A-propionate of the heme in Cyt b_{559}, these two Arg residues may be able to partially compensate each other on the electrostatic interactions with the heme propionate in Cyt b_{559} mutant cells. In contrast, the side chain of the Arg17 residue on the β-subunit of Cyt b_{559} interacts alone with the D-propionate of the heme in Cyt b_{559}. Therefore, mutation of the Arg17 residue on the β-subunit of Cyt b_{559} may have larger impacts on the structure and stability of PSII.

The R7Eα, R17Aα and R17Lβ Cyt b_{559} mutant cells showed normal S state transition by both oxygen-flash yield and TL measurements. In addition, most of these Cyt b_{559} mutant cells (except for R17Lβ mutant cells) showed similar kinetics of S_2 Q_A^- recombination compared to that of the wild-type cells. These results indicate that the Mn cluster and Q_A are generally intact in PSII of these mutant cells. Furthermore, fluorescence decay kinetics indicates slower electron transfer from Q_A to Q_B in PSII of the R7Eα and R17Lβ mutant cells. Moreover, the small down-shift of the T_{max} of B-bands in the R7Eα and R17Lβ mutant cells indicated that the equilibrium between Q_B and Q_A was slightly altered in these mutant cells. R7Eα and R17Lβ mutation may have induced a small but significant structural perturbation to the structure and redox properties of the Q_B site in PSII.

The finding that the R7Eα, R17Aα and R17Lβ PSII core complexes gave rise to high-spin signals (g~6.10 and g~5.91) is intriguing. The high spin state (S = 5/2) is believed to correspond to a five-coordinate complex of Fe^{III}PorL ([57] and the references therein). Therefore, our results indicate the displacement of one of the axial ligands to the heme of Cyt b_{559} in these mutant reaction centers. The high-spin EPR signals (g~6.10 and g~5.91) were observed previously in the R7Lα and H22Kα Cyt b_{559} mutant PSII core complexes [30,31]. Our results demonstrated that the electrostatic interactions between these Arg residues and the heme propionates of Cyt b_{559} play an important role in stability of the axial ligand ligations in the heme of Cyt b_{559}. In addition, our four-step redox titration results showed that the R7Eα and R17Lβ PSII core complexes predominantly contain the LP form of Cyt b_{559} and the R17Eα PSII core complexes contain similar amounts of IP and LP forms. In contrast, the wild-type PSII core complexes predominantly contained the IP form of Cyt b_{559}. Overall, our results demonstrate that these arginine residues on the cytoplasmic-side of Cyt b_{559} are important to the structure and redox properties of Cyt b_{559}. One previous FTIR study

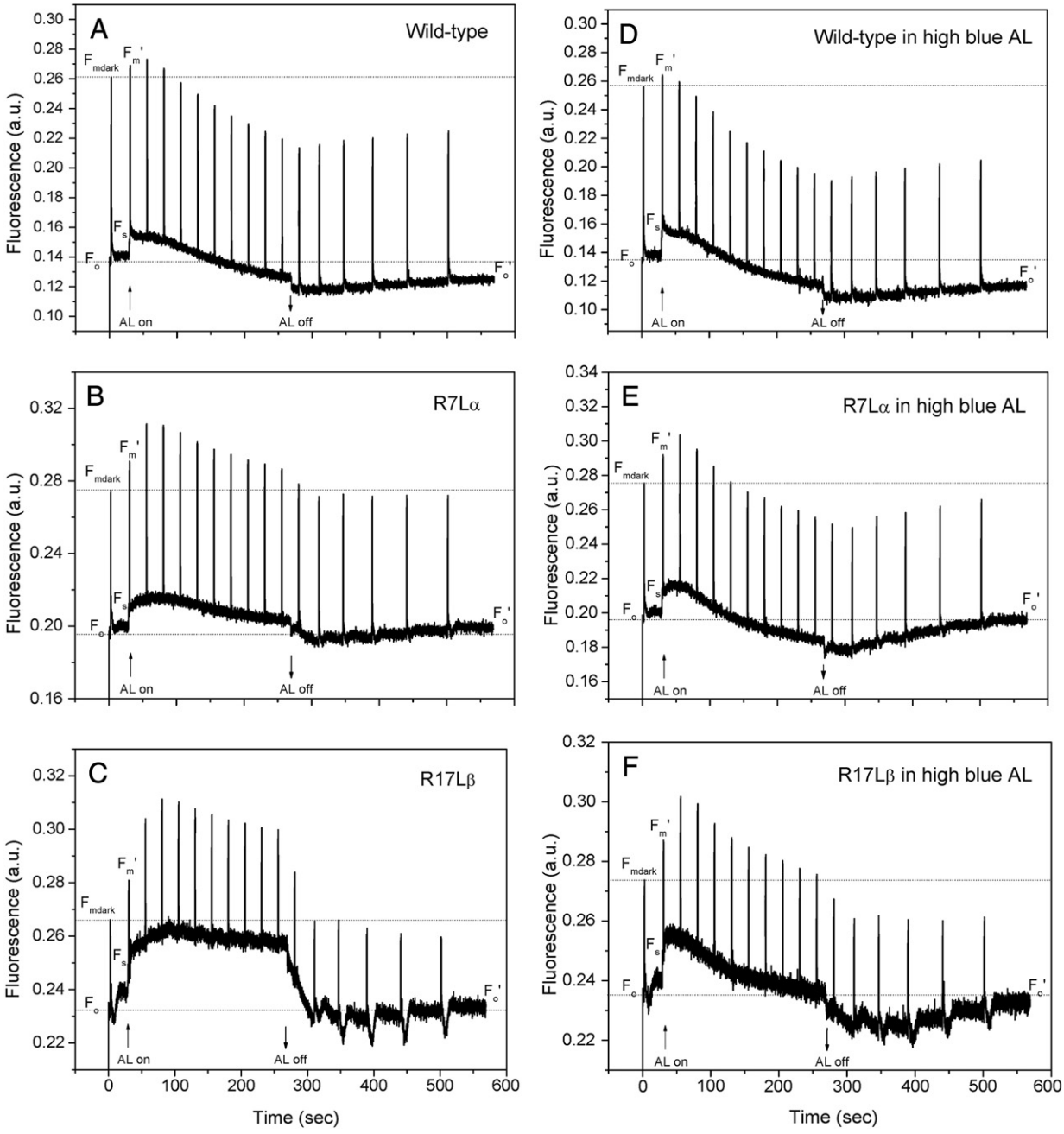

Fig. 8. Time-dependent flash-induced fluorescence yield of the wild-type (A, D), R7Lα (B, E) and R17Lβ (C, F) mutant cells in the presence and absence of high-intensity blue actinic light. The intensity of the blue actinic light was (A) to (C) ~220 μE m^{-2} s^{-1} and (D) to (F) ~350 μE m^{-2} s^{-1}. The other conditions were the same as in Fig. 7.

proposed a change in environment of one histidine ligand and a propionic group of the heme for the LP form (or IP form) of Cyt b_{559} as compared with the HP form [58]. Our results are consistent with this proposal.

An early site-directed mutagenesis study with *C. reinhardtii* showed that the Cyt b_{559} α-subunit mutants R18G and R18E had about 60% of oxygen-evolution activity as compared with wild-type cells and were sensitive to photoinhibition at high light conditions [59]. This study suggested that Arg18 played a significant role in helping Cyt b_{559} maintain the structure of the PSII complex and its activity [59]. The other site-directed mutagenesis study using *Thermosynechococcus elongatus* showed that the R18Sα Cyt b_{559} mutant cells grew photoautotrophically but were sensitive to high light [60]. In addition, R18Sα Cyt b_{559} mutant PSII preparations contained ~20% of the HP form and ~80% of the IP form of Cyt b_{559}, whereas wild-type PSII preparations contained ~85% of the HP form and ~15% of the IP form of Cyt b_{559}. The previous TL results also showed that the R18Sα Cyt b_{559} mutant cells had a decreased amount of active PSII complexes and significant alterations in the S_0/S_1 state ratio and/or redox state of PQ pool in the dark [60]. Taken together, Cyt b_{559} mutant studies [59,60 and this study] support that these arginine residues of the cytoplasmic-side of Cyt b_{559} are important in the structure and redox properties of Cyt b_{559} and the stability of PSII complexes.

4.2. Blue light-induced NPQ is altered in Cyt b_{559} mutant cells

Our findings that blue-light-induced NPQ was significantly attenuated and its recovery was accelerated in the R7Lα and R17Lβ Cyt b_{559} mutant cells were also very intriguing. To our knowledge, this is the first report on PSII reaction center mutants altering the blue-light-induced

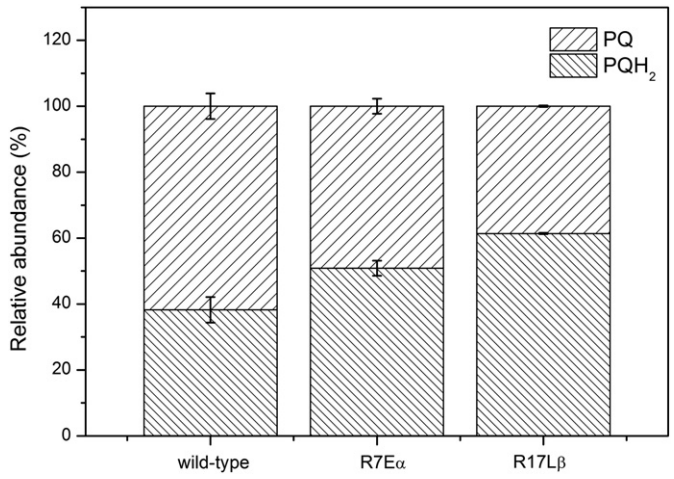

Fig. 9. UPLC-APCI-QTOFMS measurement of the redox state of the plastoquinone pool (PQ) in the wild-type, R7Eα and R17Lβ mutant cells. Samples were incubated in darkness for 10 min. The PQH_2/PQ_{tot} ratios were 0.38 ± 0.04, 0.51 ± 0.02, 0.61 ± 0.01 for the wild-type, R7Eα, and R17Lβ mutant cells, respectively.

NPQ in cyanobacteria. Previous studies have showed that orange carotenoid proteins (OCP) absorb blue light and undergo structural changes leading to the formation of a red active form ([61] and the references therein). The activated red form of OCP interacts with the phycobilisome and induces NPQ in cyanobacteria. In addition, the recovery of blue light-induced NPQ is assisted by a fluorescence recovery protein (Slr1964 gene product) in *Synechocystis* PCC6803 ([61] and the references therein). The interaction site for the OCP was proposed to be on one of the central allophycocyanin disks of the base cylinders [62,63]. On the other hand, previous studies predicted possible docking sites for the phycobilisomes on the PSII reaction centers [64,65]. The cytoplasmic side of Cyt b_{559} is located within the predicted contact sites in PSII for the APC core complex [65]. Furthermore, our previous mutant results suggest that the Arg7Leu mutation on the α-subunit of Cyt b_{559} alters the interaction between the APC core complex and PSII reaction centers, which reduces energy delivery from the antenna to the reaction center and thus protects mutant cells from DCMU-induced photo-oxidative stress [31]. Taken together, we propose that the mutation on these arginine residues of the cytoplasmic side of Cyt b_{559} may induce conformational changes that influence the interaction of the APC core complex with the OCP, thereby altering the OCP-induced NPQ and its recovery in cyanobacteria. Alternatively, the alteration of the blue light-induced NPQ effect and its recovery rate in the R7Lα and R17Lβ Cyt b_{559} mutant cells may be originated from uncoupled phycobilisomes in these mutant cells. 77 K-fluorescence results suggested that a significant fraction of phycobilisomes were uncoupled to the PSII reaction centers in the R7Lα and R17Lβ mutant cells. These uncoupled phycobilisomes may have distinct properties on the blue-light-induced NPQ which may explain our observations.

4.3. Implications for the physiological functions of Cyt b_{559}

Despite extensive studies in the last three decades, the exact function of Cyt b_{559} is still not clear. A number of proposals have aimed to explain the function of Cyt b_{559}: (1) roles in secondary electron transfers [5–10], (2) plastoquinol oxidase [11–14], (3) superoxide oxidase and reductase [17,18], (4) role in the assembly of PSII [21–27].

Several previous studies have proposed that b_{559} participates in secondary electron transfers that protect PSII from photoinhibition [5–13]. In these models, Cyt b_{559} is thought to donate its electron, via a β-carotene molecule (Car_{D2}), to reduce highly oxidized chlorophyll radicals generated in the PSII reaction centers under donor-side photoinhibitory conditions [5–10]. Our results showed that the R7Eα, and R17Lβ Cyt b_{559} mutant core complexes contained predominantly LP forms. In addition, we found no significant light-induced EPR signals for photo-oxidization of the HP or IP form of Cyt b_{559} in the R7Eα, R17Aα and R17Lβ mutant PSII core complexes under 77 K-illumination. Therefore, Cyt b_{559} in these mutant cells may have been predominantly oxidized and unable to donate its electron efficiently, via Car_{D2}, to reduce highly oxidized chlorophyll radicals generated in the PSII reaction centers under donor-side photoinhibitory conditions. In addition, whether the oxidized LP form of Cyt b_{559} in mutant cells can accept an electron from a reduced PQ on the acceptor side of PSII under acceptor-side photoinhibitory conditions is unknown. Therefore, impaired secondary electron transfer pathways in these Cyt b_{559} mutant cells may explain their high susceptibility to photo-inhibition even under growth light conditions. Our data support a functional role of Cyt b_{559} in protecting PSII under photoinhibition conditions in vivo.

Our UPLC-APCI-QTOFMS results demonstrated that the PQ pool was more reduced in the R7Eα and R17Lβ Cyt b_{559} mutant than wild-type cells in the dark. In addition, in the dark-adapted R7Eα, R17Eα and R17Lβ Cyt b_{559} mutant cells, the chlorophyll *a* fluorescence induced by a multiple-turnover saturating light pulse decayed to the F_0 level initially and then increased to a higher fluorescence level and decayed back to the F_0 (see Fig. 7). In contrast, this effect was not apparent under red actinic light or far-red light illumination (see Fig. 7 and Fig. S5). We observed the same effect in the H22Kα and Y18Sα Cyt b_{559} mutant cells [30]. A similar but much stronger effect was observed in a previous study of the ΔpsbL tobacco mutant [66]. The authors of this study attributed their results to the back electron flow from plastoquinol in the ΔpsbL tobacco mutant [66]. The back electron flow from plastoquinol to PSII enhances the formation of singlet oxygen and causes light-induced damage to PSII, which is typical of acceptor-side photoinhibition [67]. Therefore, our results suggest that Cyt b_{559} may function to ensure unidirectional forward electron flow from Q_A^- to the PQ pool. From chlorophyll *a* fluorescence and TL results, Krieger-Liszkay and co-workers demonstrated that the PQ pool was significantly over-reduced in the tobacco F26Sβ Cyt b_{559} mutant [13]. The mature leaves of the mutant showed higher susceptibility to photoinhibition and greater production of singlet oxygen [14]. The authors proposed that Cyt b_{559} may function as a PQH_2 oxidase to keep the PQ pool and the acceptor-side of PSII oxidized in the dark, which protects PSII against the acceptor-side photoinhibition [13,14]. Molecular oxygen was suggested as the terminal electron acceptor in this process [13,14]. Our results agree with this proposal.

In the 2.9 Å resolution X-ray crystallographic structural models of PSII, a novel PQ (Q_C) binding site were located in proximity to Cyt b_{559} [3]. The head group of Q_C is placed at a distance about 20 Å to the heme iron of Cyt b_{559}. The occupancy of this Q_C site by PQ was proposed to be involved in exchange of PQ on the Q_B site from the pool [3] or to modulate the redox equilibration between Cyt b_{559} and the PQ pool [3,19,20]. Particularly, the Q_C site could be the catalytic site for PQH_2 oxidase activity of Cyt b_{559} [3,18] and the switch for conversion of different redox forms of Cyt b_{559} [19,20]. However, occupancy of the Q_C site was not observed in the 1.9 Å resolution crystal structural models of PSII [1]. Future studies are needed to verify the discrepancy about the Q_C site and determine the exact Q_C function.

Previous studies showed that illumination of Tris-washed PSII membranes induced photoreduction and photooxidation of IP and HP forms of Cyt b_{559}, respectively [17,18]. It have been proposed that the IP form of Cyt b_{559} serves as superoxide oxidase (SOO) which catalyzes the oxidation of superoxide to O_2 and also that the HP form of Cyt b_{559} serves as superoxide reductase (SOR) which catalyzes the reduction of superoxide to H_2O_2. Since these arginine mutant PSII reaction centers contained predominantly LP form of Cyt b_{559}, it will be important to determine whether the SOO and SOR functions are defective in these mutant PSII reaction centers and their physiological significances.

Previous mutant studies clearly demonstrated that Cyt b_{559} was very important to the assembly and stability of the PSII reaction centers ([5]

and the references therein). For examples, among all the site-directed mutants constructed on the Cyt b_{559} heme ligands (His22 of the α- or β-subunit) with *Synechocystis* PCC6803 cells, only the H22Kα mutant grew photoautotrophically and accumulated stable PSII reaction centers [29]. In contrast, these arginine Cyt b_{559} mutant cells were able to grow photoautotrophically, assemble stable PSII reaction centers and show the normal period-four oscillation in oxygen yield. In addition, all these mutant PSII core complexes retained the heme of Cyt b_{559} and had distinct spectroscopic and redox properties. Therefore, these Cyt b_{559} mutants and their reaction centers appear suitable to study the functional roles of Cyt b_{559} in PSII. For examples, one previous FTIR study suggested the involvement of one protonated heme propionic group for the photooxidation of the LP form or IP form of Cyt b_{559} [58]. These arginine Cyt b_{559} mutants would be useful in FTIR studies to verify this proposal.

In conclusion, our data support a functional role of Cyt b_{559} in protecting PSII from the photoinactivation under photoinhibition conditions in vivo. In addition, we demonstrate that the electrostatic interactions between the cytoplasmic side arginine residues and the heme propionates of Cyt b_{559} are important to the structure and redox properties of Cyt b_{559} and the stability of PSII complexes. Future spectroscopic and function characterization of these Cyt b_{559} mutants and reaction centers will provide further insights into the physiological functions of Cyt b_{559} in PSII.

Acknowledgements

This work was supported by the National Science Council in Taiwan (NSC 99-2331-B-001 and NSC 100-2627-M-001-004) and by Academia Sinica to H.A.C. We thank the Small Molecule Metabolomics core facility in IPMB and Academia Sinica Scientific Instrument Center for helping UPLC-APCI-QTOFMS experiments.

Appendix A. Supplementary data

Supplementary data to this article can be found online at http://dx.doi.org/10.1016/j.bbabio.2013.01.016.

References

[1] Y. Umena, K. Kawakami, J.-R. Shen, N. Kamiya, Crystal structure of oxygen-evolving photosystem II at a resolution of 1.9 Å, Nature 473 (2011) 55–60.
[2] J. Kern, G. Renger, Photosystem II: structure and mechanism of the water:plastoquinone oxidoreductase, Photosynth. Res. 94 (2007) 183–202.
[3] A. Guskov, J. Kern, A. Gabdulkhakov, M. Broser, A. Zouni, W. Saenger, Cyanobacterial photosystem II at 2.9-Å resolution and the role of quinones, lipids, channels and chloride, Nat. Struct. Mol. Biol. 16 (2009) 334–342.
[4] D.H. Stewart, G.W. Brudvig, Cytochrome b_{559} of photosystem II, Biochim. Biophys. Acta Bioenerg. 1367 (1998) 63–87.
[5] K.E. Shinopoulos, G.W. Brudvig, Cytochrome b_{559} and cyclic electron transfer within photosystem II, Biochim. Biophys. Acta Bioenerg. 1817 (2011) 66–75.
[6] L.K. Thompson, G.W. Brudvig, Cytochrome *b*-559 may function to protect photosystem II from photoinhibition, Biochemistry 27 (1988) 6653–6658.
[7] C.A. Buser, B.A. Diner, G.W. Brudvig, Photo-oxidation of cytochrome b_{559} in oxygen-evolving photosystem II, Biochemistry 31 (1992) 11449–11459.
[8] C.A. Tracewell, G.W. Brudvig, Characterization of the secondary electron-transfer pathway intermediates of photosystem II containing low-potential cytochrome b_{559}, Photosynth. Res. 98 (2008) 189–197.
[9] A. Magnuson, M. Rova, F. Mamedov, P.O. Fredriksson, S. Styring, The role of cytochrome b_{559} and tyrosineD in protection against photoinhibition during *in vivo* photoactivation of photosystem II, Biochim. Biophys. Acta Bioenerg. 1411 (1999) 180–191.
[10] J. Barber, J. De Las Rivas, A functional model for the role of cytochrome b_{559} in the protection against donor and acceptor side photoinhibition, Proc. Natl. Acad. Sci. U. S. A. 90 (1993) 10942–10946.
[11] J. Kruk, K. Strzalka, Dark reoxidation of the plastoquinone-pool is mediated by the low-potential form of cytochrome *b*-559 in spinach thylakoids, Photosynth. Res. 62 (1999) 273–279.
[12] J. Kruk, K. Strzalka, Redox changes of cytochrome b_{559} in the presence of plastoquinone, J. Biol. Chem. 276 (2001) 86–91.
[13] N. Bondarava, L. De Pascalis, S. Al-Babili, C. Goussias, J.R. Golecki, P. Beyer, R. Bock, A. Krieger-Liszkay, Evidence that cytochrome b_{559} mediates the oxidization of reduced plastoquinone in the dark, J. Biol. Chem. 278 (2003) 13554–13560.
[14] N. Bondarava, C.M. Gross, M. Mubarakshina, J.R. Golecki, G.N. Johnson, A. Krieger-Liszkay, Putative function of cytochrome b_{559} as a plastoquinol oxidase, Physiol. Plant. 138 (2010) 463–473.
[15] J.M. Ortega, M. Hervás, M. Losada, Redox and acid–base characterization of cytochrome *b*-559 in photosystem II particles, Eur. J. Biochem. 171 (1988) 449–455.
[16] M. Roncel, J.M. Ortega, M. Losada, Factors determining the special redox properties of photosynthetic cytochrome b_{559}, Eur. J. Biochem. 268 (2001) 4961–4968.
[17] A. Tiwari, P. Pospisil, Superoxide oxidase and reductase activity of cytochrome b_{559} in photosystem II, Biochim. Biophys. Acta Bioenerg. 1787 (2009) 985–994.
[18] P. Pospisil, Enzymatic function of cytochrome b_{559} in photosystem II, J. Photochem. Photobiol. B 104 (2011) 341–347.
[19] O. Kaminskaya, V.A. Shuvalov, G. Renger, Evidence for a novel quinone binding site in the photosystem II complex that regulate the redox potential of cytochrome b_{559}, Biochemistry 46 (2007) 1091–1105.
[20] O. Kaminskaya, V.A. Shuvalov, G. Renger, Two reaction pathways for transformation of high potential cytochrome b_{559} of PS II into the intermediate potential form, Biochim. Biophys. Acta Bioenerg. 1767 (2007) 550–558.
[21] H.B. Pakrasi, J.G.K. Williams, C.J. Arntzen, Targeted mutagenesis of the *psb*E and *psb*F genes blocks photosynthetic electron transport: evidence for a functional role of cytochrome b_{559} in photosystem II, EMBO J. 7 (1988) 325–332.
[22] H.B. Pakrasi, B.A. Diner, J.G.K. Williams, C.J. Arntzen, Deletion mutagenesis of the cytochrome b_{559} protein inactivates the reaction center of photosystem II, Plant Cell 1 (1989) 591–597.
[23] H.B. Pakrasi, K.J. Nyhus, H. Granok, Targeted deletion mutagenesis of the β subunit of cytochrome b_{559} protein destabilizes the reaction center of photosystem II, Z. Naturforsch. 45c (1990) 423–429.
[24] F. Morais, J. Barber, P.J. Nixon, The chloroplast-encoded α subunit of cytochrome b_{559} is required for assembly of the photosystem two complex in both the light and the dark in *Chlamydomonas reinhardtii*, J. Biol. Chem. 273 (1998) 29315–29320.
[25] M. Swiatek, R.E. Regel, J. Meurer, G. Wanner, H.B. Pakrasi, I. Ohad, R.G. Herrmann, Effects of selective inactivation of individual genes for low-molecular-mass subunits on the assembly of photosystem II, as revealed by chloroplast transformation: the *psb*EFLJ operon in *Nicotiana tabacum*, Mol. Genet. Genomics 268 (2003) 699–710.
[26] M. Suorsa, R.E. Regel, V. Paakkarinen, N. Battchikova, R.G. Herrmann, E.M. Aro, Protein assembly of photosystem II and accumulation of subcomplexes in the absence of low molecular mass subunits *psb*L and *psb*J, Eur. J. Biochem. 271 (2004) 96–107.
[27] H.B. Pakrasi, P. De Ciechi, J. Whitmarsh, Site-directed mutagenesis of the heme axial ligands of cytochrome b_{559} affects the stability of the photosystem II complex, EMBO J. 10 (1991) 1619–1627.
[28] F. Morais, K. Kuhn, D.H. Stewart, J. Barber, G.W. Brudvig, P.J. Nixon, Photosynthetic water oxidation in cytochrome b_{559} mutants containing a disrupted heme-binding pocket, J. Biol. Chem. 276 (2001) 31986–31993.
[29] C.H. Hung, J.Y. Huang, Y.F. Chiu, H.A. Chu, Site-directed mutagenesis on the heme axial-ligands of cytochrome b_{559} in photosystem II by using cyanobacteria *Synechocystis* PCC 6803, Biochim. Biophys. Acta Bioenerg. 1767 (2007) 686–693.
[30] C.H. Hung, H.J. Hwang, Y.H. Chen, Y.F. Chiu, S.C. Ke, R.L. Burnap, H.A. Chu, Spectroscopic and functional characterizations of cyanobacterium *Synechocystis* PCC 6803 mutants on and near the heme axial ligand of cytochrome b_{559} in photosystem II, J. Biol. Chem. 285 (2010) 5653–5663.
[31] Y.F. Chiu, W.C. Lin, C.M. Wu, Y.H. Chen, C.H. Hung, S.C. Ke, H.-A. Chu, Identification and characterization of a cytochrome b_{559} *Synechocystsis* 6803 mutant spontaneously generated from DCMU-inhibited photoheterotrophical growth conditions, Biochim. Biophys. Acta Bioenerg. 1787 (2009) 1179–1188.
[32] H.-A. Chu, A.P. Nguyen, R.J. Debus, Site-directed photosystem II mutants with perturbed oxygen-evolving properties. 1. Instability or inefficient assembly of the manganese cluster *in vivo*, Biochemistry 33 (1994) 6137–6149.
[33] J.M. Ducruet, Chlorophyll thermoluminescence of leaf discs: simple instruments and progress in signal interpretation open the way to new ecophysiological indicators, J. Exp. Bot. 54 (2003) 2419–2430.
[34] J.L. Zurita, M. Roncel, M. Aguilar, J.M. Ortega, A thermoluminescence study of Photosystem II back electron transfer reactions in rice leaves—effects of salt stress, Photosynth. Res. 84 (2005) 131–137.
[35] J.M. Ducruet, A. Serrano, M. Roncel, J.M. Ortega, Peculiar properties of chlorophyll thermoluminescence emission of autotrophically or mixotrophically grown *Chlamydomonas reinhardtii*, J. Photochem. Photobiol. B 104 (2011) 301–307.
[36] J.M. Ducruet, T. Miranda, Graphical and numerical analysis of thermoluminescence and fluorescence F_0 emission in photosynthetic material, Photosynth. Res. 33 (1992) 15–27.
[37] R.L. Burnap, M. Qian, C. Pierce, The manganese stabilizing protein (MSP) of photosystem II modifies the in vivo deactivation and photoactivation kinetics of the H_2O-oxidation complex in *Synechocystis* sp. PCC6803, Biochemistry 35 (1996) 874–882.
[38] P.C. Meunier, R.L. Burnap, L.A. Sherman, Modelling of the S-state mechanism and Photosystem II manganese photoactivation in cyanobacteria, Photosynth. Res. 47 (1995) 61–76.
[39] M. Qian, L. Dao, R.J. Debus, R.L. Burnap, Impact of mutations within the putative Ca^{2+}-binding lumenal interhelical a–b loop of the photosystem II D1 protein on the kinetics of photoactivation and H_2O-oxidation in *Synechocystis* sp. PCC6803, Biochemistry 38 (1999) 6070–6081.
[40] P.J. Nixon, B.A. Diner, Aspartate 170 of the photosystem II reaction center polypeptide D1 is involved in the assembly of the oxygen evolving manganese cluster, Biochemistry 31 (1992) 942–948.
[41] J. Martinis, F. Kessler, G. Glauser, A novel method for prenylquinone profiling in plant tissues by ultra-high pressure liquid chromatography–mass spectrometry, Plant Methods 7 (2011) 23.

[42] F. Rappaport, M. Guergova-Kuras, P.J. Nixon, B.A. Diner, J. Lavergne, Kinetics and pathways of charge recombination in photosystem II, Biochemistry 41 (2002) 8518–8527.
[43] R. de Wijn, H.J. van Gorkom, Kinetics of electron transfer from Q(A) to Q(B) in photosystem II, Biochemistry 40 (2001) 11912–119222.
[44] Y. Allahverdiyeva, Z. Deák, A. Szilárd, B.A. Diner, P.J. Nixon, I. Vass, The function of D1-H332 in Photosystem II electron transport studied by thermoluminescence and chlorophyll fluorescence in site-directed mutants of *Synechocystis* 6803, Eur. J. Biochem. 271 (2004) 3523–3532.
[45] M. Roncel, J.M. Ortega, Afterglow thermoluminescence band as a possible early indicator of changes in the photosynthetic electron transport in leaves, Photosynth. Res. 84 (2005) 167–172.
[46] J.M. Ducruet, I. Vass, Thermoluminescence: experimental, Photosynth. Res. 101 (2009) 195–204.
[47] J. Lavorel, Matrix analysis of the oxygen evolving system of photosynthesis, J. Theor. Biol. 57 (1976) 171–185.
[48] P.C. Meunier, R.L. Burnap, L.A. Sherman, Improved 5-step modeling of the Photosystem II S-state mechanism in cyanobacteria, Photosynth. Res. 47 (1995) 61–76.
[49] G. AjLani, G. Vernotte, L. DiMagno, R. Haselkorn, Phycobilisome core mutants of *Synechocystis* PCC6803, Biochim. Biophys. Acta Bioenerg. 1231 (1995) 189–196.
[50] V.A. Dzelzkalns, L. Bogorad, Spectral properties and composition of reaction center and ancillary polypeptide complexes of photosystem II deficient mutants of *Synechocystis* 6803, Plant Physiol. 90 (1989) 617–623.
[51] G. Ajlani, C. Vernotte, Functional analysis of the two homologous psbA gene copies in *Synechocystis* PCC 6714 and PCC 6803, Plant Mol. Biol. 37 (1998) 577–580.
[52] E. Haag, J.J. Eaton-Rye, G. Renger, W.F.J. Vermaas, Functionally important domains of the large hydrophilic loop of CP47 as probed by oligonucleotide-directed mutagenesis in *Synechocystis* sp. PCC 6803, Biochemistry 32 (1993) 4444–4454.
[53] D. Bruce, S. Brimble, D.A. Bryant, State transitions in a phycobilisome-less mutant of the cyanobacterium *Synechococcus* sp. PCC 7002, Biochim. Biophys. Acta Bioenerg. 974 (1989) 66–73.
[54] K. Kondo, C.W. Mullineaux, M. Ikeuchi, Distinct roles of CpcG1-phycobilisome and CpcG2-phycobilisome in state transitions in a cyanobacterium *Synechocystis* sp. PCC 6803, Photosynth. Res. 99 (2009) 217–225.
[55] F. Müh, T. Renger, A. Zouni, Crystal structure of cyanobacterial photosystem II at 3.0 Å resolution: a closer look at the antenna system and the small membrane-intrinsic subunits, Plant Physiol. Biochem. 46 (2008) 238–264.
[56] G.R. Moore, D.E. Harris, F.A. Leitch, G.W. Pettigrew, Characterization of ionisations that influence the redox potential of mitochondrial cytochrome c and photosynthetic bacterial cytochromes c_2, Biochim. Biophys. Acta Bioenerg. 764 (1984) 331–342.
[57] T.N. Kropacheva, W.O. Feikema, F. Mamedov, Y. Feyziyev, S. Styring, A.J. Hoff, Spin conversion of cytochrome b_{559} in photosystem II induced by exogenous high potential quinine, Chem. Phys. 294 (2003) 471–482.
[58] C. Berthomieu, A. Boussac, W. Mäntele, J. Breton, E. Nabedryk, Molecular changes following oxidoreduction of cytochrome b_{559} characterized by Fourier transform infrared difference spectroscopy and electron paramagnetic resonance: photooxidation in photosystem II and electrochemistry of isolated cytochrome b_{559} and iron protoporphyrin IX-bisimidazole model compounds, Biochemistry 31 (1992) 11460–11471.
[59] J.J. Ma, L.B. Li, Y.X. Jing, T.Y. Kuang, Mutation of residue Arginine 18 of cytochrome b_{559} α-subunit and its effect on photosystem II activity in *Chlamydomonas reinhardtii*, J. Integr. Plant Biol. 49 (2007) 1054–1061.
[60] F. Guerrero, M. Roncel, D. Kirilovsky, J.M. Ortega, Site-directed mutagenesis of cytochrome b_{559} in the cyanobacterium *Thermosynechococcus elongatus*, in: J.F. Allen, E. Gantt, J.H. Golbeck, B. Osmond (Eds.), Photosynthesis. Energy from the Sun: 14th International Congress on Photosynthesis, Springer, Dordrecht, The Netherlands., 2008, pp. 15–18.
[61] D. Kirilovsky, C.A. Kerfeld, The orange carotenoid protein in photoprotection of photosystem II in cyanobacteria, Biochim. Biophys. Acta Bioenerg. 1817 (2012) 158–166.
[62] D. Jallet, M. Gwizdala, D. Kirilovsky, ApcD, ApcF and ApcE are not required for the Orange Carotenoid Protein related phycobilisome fluorescence quenching in the cyanobacterium *Synechocystis* PCC 6803, Biochim. Biophys. Acta Bioenerg. 1817 (2012) 1418–1427.
[63] I.N. Stadnichuk, M.F. Yanyushin, E.G. Maksimov, E.P. Lukashev, S.K. Zharmukhamedov, I.V. Elanskaya, V.Z. Paschenko, Site of non-photochemical quenching of the phycobilisome by orange carotenoid protein in the cyanobacterium *Synechocystis* sp. PCC 6803, Biochim. Biophys. Acta Bioenerg. 1817 (2012) 1436–1445.
[64] D. Bald, J. Kruip, M. Rögner, Supramolecular architecture of cyanobacterial thylakoid membranes: how is the phycobilisome connected with the photosystem? Photosynth. Res. 49 (1996) 103–118.
[65] J. Barber, E.P. Morris, P.C.A. da Fonseca, Interaction of allophycocyanin core complex with photosystem II, Photochem. Photobiol. Sci. 2 (2003) 536–541.
[66] I. Ohad, C. Dal Bosco, R.G. Herrmann, J. Meurer, Photosystem II proteins PsbL and PsbJ regulate electron flow to the plastoquinone pool, Biochemistry 43 (2004) 2297–2308.
[67] A.W. Rutherford, A. Krieger-Liszkay, Herbicide-induced oxidative stress in photosystem II, Trends Biochem. Sci. 26 (2001) 648–653.